On the Stability of Full Adaptive Observer for Induction Motor in Regenerating Mode

Erik Etien, Claude Chaigne, and Nadia Bensiali

Abstract—**This paper, which deals with the stability of adaptive observers for induction motor in the regenerating mode, proposes a new approach that is consist of describing the error system in state space representation. With this formulation, it is possible to establish a cartography of unstable eigenvalues in the torque/speed plane, thus simplifying the stability analysis. Moreover, a new stability criterion is defined and used to realize stabilizing designs based on feedback gain as well as on the speed adaptation law.**

Index Terms—**Induction motor drives, observers, regenerating mode, stability.**

NOMENCLATURE

$\underline{i}_s = i_{sd} + ji_{sq}$	Stator current space vector.
$\underline{\psi}_R = \psi_{rd} + j\psi_{rq}$	Rotor flux space vector.
ψ_{ref}	Rotor flux modulus reference.
ω_{sl}	Slip frequency.
ω	Electrical rotor speed.
$\omega_s = \omega_{\text{sl}} + \omega$	Stator frequency.
R_s	Stator resistance.
R_R	Rotor resistance.
L_M	Magnetizing inductance.
L_σ	Leakage inductance.

I. INTRODUCTION

STABILITY of initial full adaptive observers in regenerating mode is now a well-known problem [1], [2]. Since the early 90s, many solutions have been proposed based on stabilizing feedback gains [3]–[6], adaptation laws [7], [8], or gains/laws association [9]. These designs are generally the result of a stability study based on Routh–Hurwitz criterion applied to a transfer function representation of errors. However, each solution seems to be a particular case, and no general analysis is discussed. However, recently, efforts have been made in this direction [10]–[12]. In [10], the Lyapunov function leading to the speed adaptation law is considered in a more general form, and authors concluded that probably no solution to stability problem can be found. In [11], a common framework based on the positive real property is proposed, and design rules for the feedback and adaptation gains are defined. In [12], the link between reduced and full observers is made, and the concept of *complete stability* is introduced. This leads to stability conditions, taking feedback gain and adaptation law parameters into account. This method is very efficient in checking the influence of feedback gains and/or speed adaptation law parameters on stability. In this paper, the stability problem is tackled using a state representation, which leads to a simplified analysis. In Section II, models used in this paper are presented, and a cartography of unstable eigenvalues (UEVs) in the torque/speed plane (mapping method) is derived. It can be noted that mapping has been used in previous works in order to study combined controller/observer stability [13]. In this paper, only observer stability is investigated, and the main experimental results are implemented in a sensored control. From the state representation, the simplified instability criterion can be easily derived, and analytic expressions of stability limits are found. Then, a new interpretation of the stabilization process consists of reducing the instability area to the unobservability line $\omega_s = 0$ is presented as the main contribution of this paper. Our approach avoids using the Routh–Hurwitz analysis [12] or Lyapunov inequality [11], which can be difficult to use in the case of uncertainties in parameters for example. Although the problem of the parameter variations is not addressed in this paper, the proposed method seems to be a powerful tool for the stability analysis in this case. In Section III, two feedback gain designs leading to an unstable region reduced to the unobservability line $\omega_s = 0$ are studied. In Section IV, the design of the speed adaptation law is discussed. In this case, another solution leading to the reduced unstable region is again given and compared with previous designs through simulations and experimental results.

II. STABILITY ANALYSIS OF CLASSICAL FULL ADAPTIVE OBSERVER

A. Linearized Model

The induction motor model is described by the following state equations in the synchronous rotating reference frame and using complex notations:

$$\begin{cases} \frac{d}{dt}\underline{i}_s = -\left(\frac{1}{\tau'_\sigma} + j\omega_s\right)\underline{i}_s + \frac{1}{L_\sigma}\left(\frac{1}{\tau_R} - j\omega\right)\underline{\psi}_R + \frac{1}{L_\sigma}\underline{u}_s \\ \frac{d}{dt}\underline{\psi}_R = R_R\underline{i}_s - \left(\frac{1}{\tau_R} + j\omega_{s_l}\right)\underline{\psi}_R \end{cases}$$

$$(1)$$

with $\tau'_\sigma = (L_\sigma/(R_R + R_s))$ and $\tau_R = (L_M/R_R)$.

The classical full adaptive observer is expressed as

$$
\begin{cases}
\dfrac{d}{dt}\widehat{\underline{i}}_s = -\left(\dfrac{1}{\widehat{\tau}'_\sigma} + j\omega_s\right)\widehat{\underline{i}}_s + \dfrac{1}{\widehat{L}_\sigma}\left(\dfrac{1}{\widehat{\tau}_R} - j\widehat{\omega}\right)\widehat{\underline{\psi}}_R \\
\qquad + \dfrac{1}{\widehat{L}_\sigma}\underline{u}_s + G_s\underline{e}_i \\
\dfrac{d}{dt}\widehat{\underline{\psi}}_R = \widehat{R}_R\widehat{\underline{i}}_s - \left(\dfrac{1}{\widehat{\tau}_R} + j\widehat{\omega}_{s_l}\right)\widehat{\underline{\psi}}_R + G_r\underline{e}_i \\
\dfrac{d}{dt}\widehat{\omega} = -K_i\epsilon - K_p\dfrac{d}{dt}\epsilon
\end{cases}
\tag{2}
$$

where $\epsilon = \Im\{e^{-j\phi}\underline{e}_i\widehat{\underline{\psi}}_R^*\}$, $\underline{e}_i = (\underline{i}_s - \widehat{\underline{i}}_s)$, $G_s = \begin{bmatrix} g_{sd} & -g_{sq} \\ g_{sq} & g_{sd} \end{bmatrix}$,

and $G_r = \begin{bmatrix} g_{rd} & -g_{rq} \\ g_{rq} & g_{rd} \end{bmatrix}$. The superscript * stands for complex conjugate. The complex number $e^{-j\phi}$ is traditionally added to obtain stable behavior in regenerating mode with a correct tuning of the angle ϕ [14]. In [1], considering $\phi = 0$, the classical speed adaptation law was obtained from Lyapunov theory using the following assumption:

$$
\begin{cases}
\widehat{\underline{\psi}}_R \to \underline{\psi}_R \\
\dfrac{d}{dt}\omega = 0.
\end{cases}
\tag{3}
$$

According to (3), the set of equations in (1) can be written as

$$
\begin{cases}
\dfrac{d}{dt}\underline{i}_s = -\left(\dfrac{1}{\tau'_\sigma} + j\omega_s\right)\underline{i}_s + \dfrac{1}{L_\sigma}\left(\dfrac{1}{\tau_R} - j\omega\right)\underline{\psi}_R + \dfrac{1}{L_\sigma}\underline{u}_s \\
\dfrac{d}{dt}\underline{\psi}_R = R_R\underline{i}_s - \left(\dfrac{1}{\tau_R} + j\omega_{s_l}\right)\underline{\psi}_R \\
\dfrac{d}{dt}\omega = 0.
\end{cases}
\tag{4}
$$

By subtracting (1) to (2), the error vector $\underline{e} = [\underline{e}_i \quad \underline{e}_\psi \quad e_\omega]^T$ is defined with $\underline{e}_i = (\underline{i}_s - \widehat{\underline{i}}_s)$, $\underline{e}_\psi = (\underline{\psi}_R - \widehat{\underline{\psi}}_R)$, and $e_\omega = (\omega - \widehat{\omega})$. The estimated rotor flux is assumed to be correctly controlled and satisfy $\widehat{\psi}_{Rd0} = \psi_{\text{ref}}$ (the subscript 0 stands for the operating-point quantities). By linearizing the resulting system ($\underline{e} = \underline{e}_0 + \delta\underline{e}$) and expressing in a component form, a linearized model is defined by

$$
\dot{\delta\underline{e}} = \widehat{A}_1\delta\underline{e} + B_1\delta\underline{u}_1
\tag{5}
$$

where $\delta\underline{e} = [\delta e_{id} \quad \delta e_{iq} \quad \delta e_{\psi_d} \quad \delta e_{\psi_q} \quad \delta e_\omega]^T$ and $\delta u_1 = [\delta\omega_s \quad \delta\omega]^T$. Matrices $\widehat{A}_1$ and $\widehat{B}_1$ are given in (38) at the end of this paper, under the assumption of known parameters.

It is well known that, when $G_s = G_r = 0$ and $\phi = 0$, this observer is unstable in the regenerating mode. In the following, it is shown that this property is easily verified using state space representation.

B. Unstable Regions

1) UEVs localization: The stability of the system in (5) can be studied by defining set (D) containing the UEVs of the matrix $\widehat{A}_1$. Unstable regions in the plane $\{\omega_0, \omega_{\text{sl0}}\}$ can also be highlighted providing a powerful tool for stability analysis. The domain (D) of unstable EV is defined by

$$
D^{(\omega_0, \omega_{\text{sl0}})} = \left\{\lambda_i\left(\widehat{A}_1(\omega_0, \omega_{\text{sl0}})\right) \middle/ \Re\left\{\lambda_i\left(\widehat{A}_1(\omega_0, \omega_{\text{sl0}})\right)\right\} \geq 0\right\}.
\tag{6}
$$

TABLE I
PARAMETERS OF 1.1-kW FOUR-POLE 400-V 50-Hz MOTOR AND LOAD

Stator resistance R_s	10.75Ω
Rotor resistance R_R	3.62Ω
Magnetizing inductance L_M	$420mH$
Leakage inductance L_σ	$60mH$
Total moment of inertia	$0.040kg.m^2$
Rated speed	$1470r/mn$
Rated current	$2.6A$
Rated torque	$7N.m$

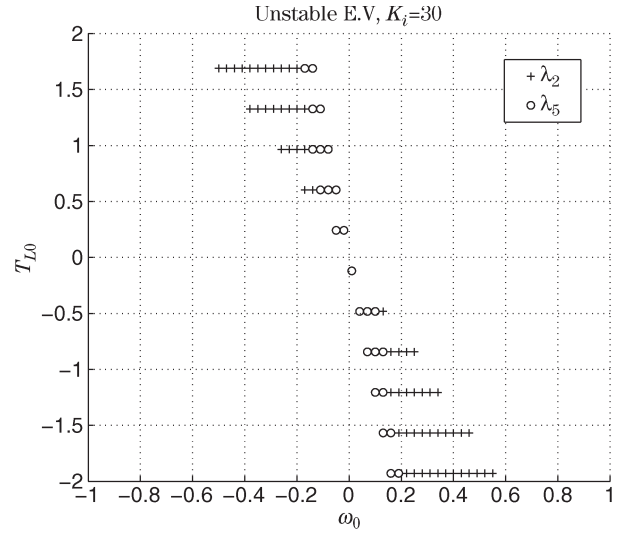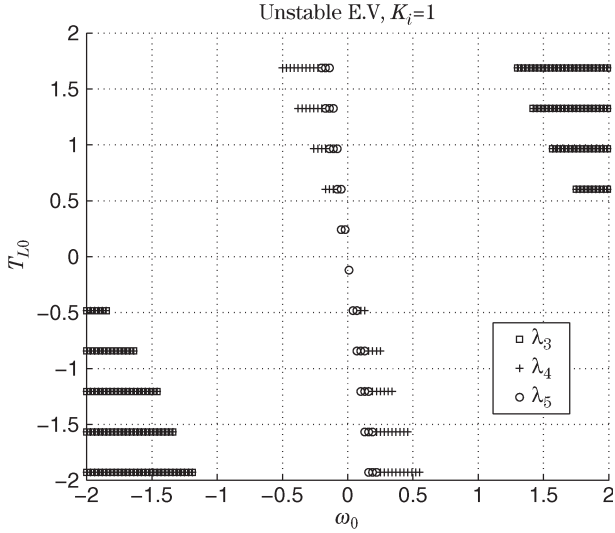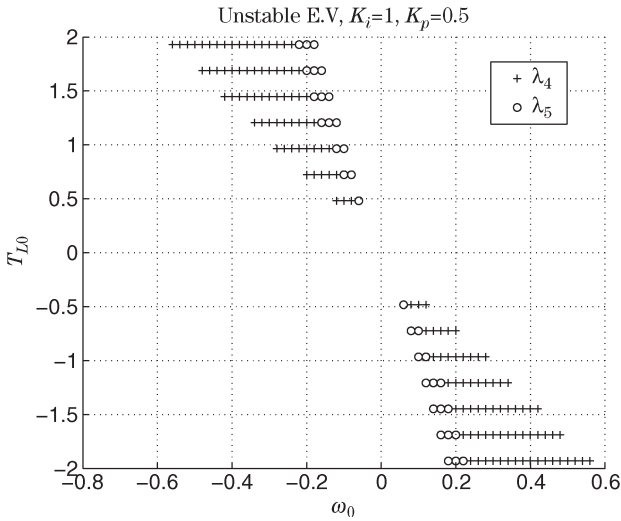

Fig. 1. Unstable EV in the $\{\omega_0, T_{L0}\}$ plane: $K_i = 30$ and $G_r = 0$.

Regions of unstable EVs can be plotted in the $\{\omega_0, \omega_{\text{sl0}}\}$ plane or in the $\{\omega_0, T_{L0}\}$ using the relationship $T_{L0} = (P\psi_{\text{ref}}^2\omega_{\text{sl0}}/R_R)$. As illustrated, let us consider the induction motor whose parameters are shown in Table I. For the classical observer corresponding to the particular case $G_s = G_r = 0$, $\phi = 0$, $K_p = 0$ [1], and $K_i = 30$, unstable EVs are λ_2 and λ_5, as shown in Fig. 1 (in all graphs, values appear in per unit). Two well-known unstable regions in the regenerating mode are highlighted. It can be noted that each part of this region is allocated to one unstable EV: λ_2 is never unstable in the same operating point as that of λ_5. This property will be used in the following sections.

For a smaller value $K_i = 1$ (see Fig. 2), unstable regions in the regenerating mode are identical, but EVs that compose these regions are different (λ_4 and λ_5 in this case). Consequently, changing parameter K_i does not affect the region localization in the $\{\omega_0, T_{L0}\}$ plane, but only the EVs repartition inside. Furthermore, two unstable regions appear in the motoring mode. Too small values for the parameter K_i can lead to unstable behavior in the motoring mode even around the nominal operating point. Now, let us consider the influence of the parameter K_p. With $K_p \neq 0$, the last row of the matrix in (38) becomes

$$
\widehat{A}_1(5,:) = \left[-K_p\omega_{s0}\psi_{\text{ref}} \quad \left(K_i - \dfrac{K_p}{\tau'_\sigma}\right)\psi_{\text{ref}} \right.
$$
$$
\left. -\dfrac{(K_p\omega_0\psi_{\text{ref}})}{L_\sigma} \quad \dfrac{K_p\psi_{\text{ref}}}{\tau_R L_\sigma} \quad -\dfrac{K_p\psi_{\text{ref}}}{L_\sigma}\right].
\tag{7}
$$

Fig. 2. Unstable EV in the $\{\omega_0, T_{L0}\}$ plane: $K_i = 1$ and $G_s = G_r = 0$.

Fig. 3. Unstable EV in the $\{\omega_0, T_{L0}\}$ plane: $K_i = 1$, $K_p = 0.5$, and $G_s = G_r = 0$.

As shown in Fig. 3, the proportional term K_p allows elimination of the unstable regions in the motoring mode without modifying the repartition of unstable EVs in the regenerating mode.

2) Relationship With Complete Stability: Harnefors and Hinkannen [12] have established some analogies between reduced and adaptive observers. It allows the determination, with correct hypothesis, of the complete stability conditions for all operating points $\{\widehat{\omega}_0, \omega_{sl0}\}$, including the regenerating mode. Obviously, the case $\omega_{s0} = 0$ must be kept apart. A completely stable observer must verify both conditions in (39), shown at the end of this paper. In fact, complete stability and UEV localization are two equivalent approaches. On one hand, conditions in (39) are calculated for ω_0 varying from -0.2 p.u. to 0 and ω_{sl0} varying from 0 to 0.08 p.u. Each couple $\{\omega_0, \omega_{sl0}\}$, which leads to unstable results of $l_1 < 0$ and $l_2 < 0$, is plotted in the $\{\omega_0, T_{L0}\}$ plane in Fig. 4. On the other hand, UEVs are directly calculated from (38) and plotted in the same figure. Both methods lead to the same results except for the upper limit of the
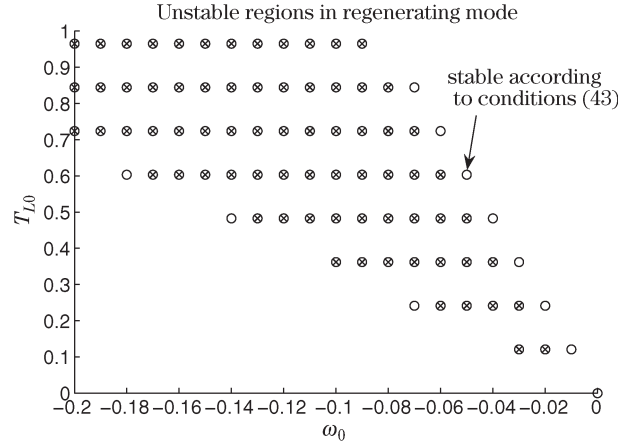
Fig. 4. Unstable regions in the $\{\omega_0, T_{L0}\}$ plane: $K_i = 1$, $K_p = 0$, $G_s = G_r = 0$, and $\phi = 0$. Markers "o" corresponding to UEV calculation and markers "x" stemmed from conditions in (39).

domain. As shown in the following, this limit, which is defined by $\omega_{s0} = 0$, corresponds to null EVs which are not considered as unstable in both conditions in (39). However, with the state space representation, it is possible to find which EV is unstable for a particular operating point. In the complete stability approach, the stability is gathered in both terms l_1 and l_2.

In this section, it is shown that, by expressing the error system (5) in state space representation, the stability can be studied by plotting UEVs in the $\{\omega_0, T_{L0}\}$ plane. This approach is different from the classical methodology using transfer function representations associated with the Routh–Hurwitz criterion and leads to a simplified analysis. With this tool, several methods for the determination of analytical expressions of stability limits (Section II-C) or observer designs (Sections III and IV) can be investigated.

C. Determination of Unstable Regions' Analytical Expressions

This section shows how the state space representation can be used to establish analytical expressions of stability limits for the system in (5). To achieve this, the sign of the determinant $\det(\widehat{A}_1)$ is expressed considering the property

$$\det(\widehat{A}_1) = \prod_{i=1}^{5} \lambda_i. \tag{8}$$

The system will be stable if all the five EVs have negative real parts. One consequence is that the instability can be proved if

$$\det(\widehat{A}_1) > 0. \tag{9}$$

The study of the sign gives a good indication on the area of instability. However, the inverse condition $\det(\widehat{A}_1) < 0$ does not imply stability because some EV values can change sign simultaneously. Considering Fig. 2, the proposed instability criterion (9) can be used in the regenerating region where no EVs change sign simultaneously. However, in the motoring region, EVs λ_3 and λ_4 are unstable for the same operating point. In this case, the sign of $\det(\widehat{A}_1)$ will not change: In this region, the criterion is not efficient.
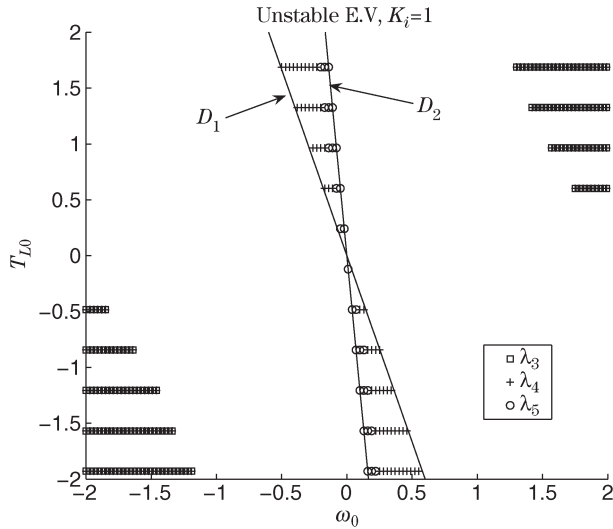
Fig. 5. Unstable EV in the $\{\omega_0, T_{L0}\}$ plane: $K_i = 1$, $K_p = 0$, and $G_s = G_r = 0$.

Now, the proposed criterion is used to find stability limits in the regenerating mode defined by $\det(\widehat{A}_1) = 0$. This leads to

$$\det(\widehat{A}_1) = -\frac{K_i \psi_{\text{ref}}^2}{L_M L_\sigma^2} \omega_{s0} [L_M R_s \omega_{sl0} + R_R (L_M + L_\sigma) \omega_{s0}] = 0. \tag{10}$$

Both solutions are

$$\begin{cases} \omega_{s0} = 0 \quad \text{or} \\ \omega_{s0} = \omega_0 \frac{1}{1 + \frac{R_R L_\sigma}{L_M R_s} + \frac{R_R}{R_s}}. \end{cases} \tag{11}$$

These solutions can be expressed in terms of ω_0 and T_{L0}

$$\begin{cases} T_{L0} = -P \frac{\psi_{\text{ref}}^2}{R_R} \omega_0 \quad \text{noted } (D_2), \text{inobservability line} \\ T_{L0} = -P \frac{\psi_{\text{ref}}^2}{R_R} \left(\frac{\frac{R_R L_\sigma}{L_M R_s} + \frac{R_R}{R_s}}{1 + \frac{R_R L_\sigma}{L_M R_s} + \frac{R_R}{R_s}} \right) \omega_0 \quad \text{named } (D_1). \end{cases} \tag{12}$$

These two lines are shown in Fig. 5 and define the limits of unstable regions in the regenerating mode but not in the motoring mode. Also, Fig. 3 shows that unstable regions are not modified by adding the proportional gain K_p in the speed adaptation law. It can be verified by seeking the conditions which lead to $\det(\widehat{A}_1) = 0$ when the last row of (38) is replaced by (7). The calculation yields to the result in (10) confirming that unstable regions in the regenerating mode are not influenced by the gain K_p.

In order to illustrate this design, a classical rotor field oriented control (RFOC) (see Fig. 6) is simulated with a 1.1-kW four-pole induction motor whose parameters are given in Table I.

The rotor speed is kept constant at a small value, and at steady state, the load torque is increased with a slow ramp from 0 to 1.5 p.u. in 20 s. Fig. 7 shows the simulation results obtained with the classical open loop observer ($G_s = 0$ and $G_r = 0$). As expected, the actual speed diverges from reference inside the region defined by D_1 and D_2. The same test is made in
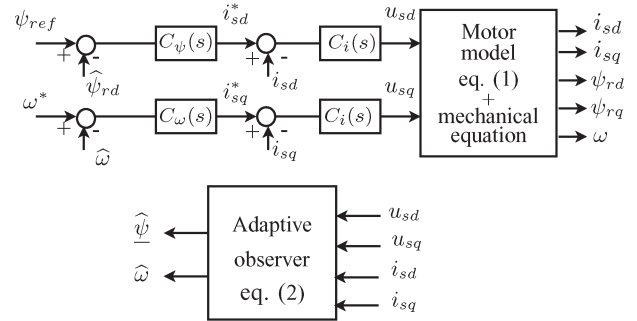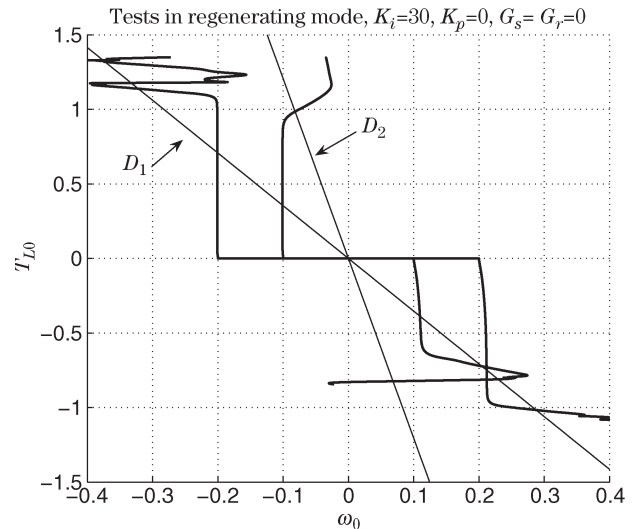

Fig. 6. Block diagram of sensorless RFOC IM simulator.

Fig. 7. Simulation results. Test in the regenerating mode in the $\{\omega_0, T_{L0}\}$ plane: $K_i = 1$, $K_p = 0$, and $G_s = G_r = 0$. Rotor speed is kept constant: $\omega_0 = -0.1$ and $\omega_0 = -0.2$ (quadrant 2) and $\omega_0 = +0.1$ and $\omega_0 = +0.2$ (quadrant 4). Ramp of load torque from 0 to 1.5 (quadrant 2) and from 0 to -1 (quadrant 4) during 20 s.

the fourth quadrant ($\omega_0 > 0$ and $T_{L0} < 0$) with similar result. Experimental tests are presented to validate simulations. The 1.1-kW four-pole induction motor (see Table I) is fed by a frequency converter controlled by a dSpace DS1104 PPC/DSP board. The measured rotor speed is used as a feedback signal for the control. The observer is simulated independently, and estimated variables are not used for the RFOC. Results are shown in Figs. 8 and 9 and confirm that the observer is unstable in the regenerating mode.

Expressions in (12) are similar to those defined in [4] and [8] where transfer functions on a five-parameter model are used. The state space representation simplifies the stability analysis and allows finding solutions for the stabilization of the observer, as shown in Sections III and IV.

In the following, the stabilization is interpreted as the reduction of the unstable region defined by D_1 and D_2. By examining the relationship in (12), it can be noted that (D_2), which is defined by $\omega_{s0} = 0$, is equivalent to the inobservability line. Then, the well-known inobservability condition defined for the motor model (1) is transformed into the stability condition for the error system in (5). The line D_2 translates an intrinsic property of the motor which cannot be influenced by the observer design. However, the line D_1 depends on observer parameters and can
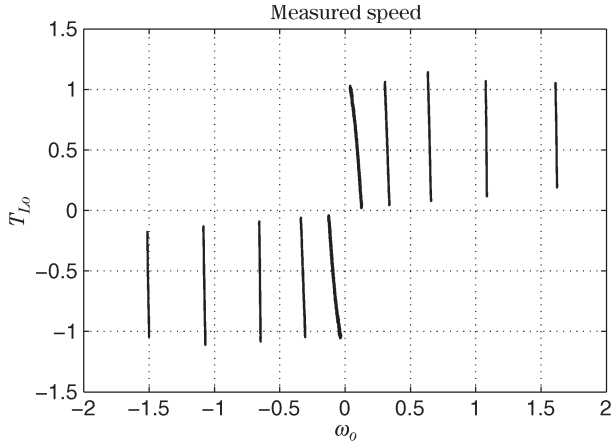
Fig. 8. Experimental results. Test in the motoring mode in the $\{\omega_0, T_{L0}\}$ plane: $K_i = 1$, $K_p = 0$, and $G_s = G_r = 0$. Rotor speed is kept constant: $\omega_0 = -0.05, -0.2, -0.6, -1$, and -1.5 (quadrant 3) and $\omega_0 = +0.05, +0.2, +0.6, +1$, and $+1.5$ (quadrant 1). Ramp of load torque from 0 to 1 (quadrant 1) and from 0 to -1 (quadrant 3) during 100 s.
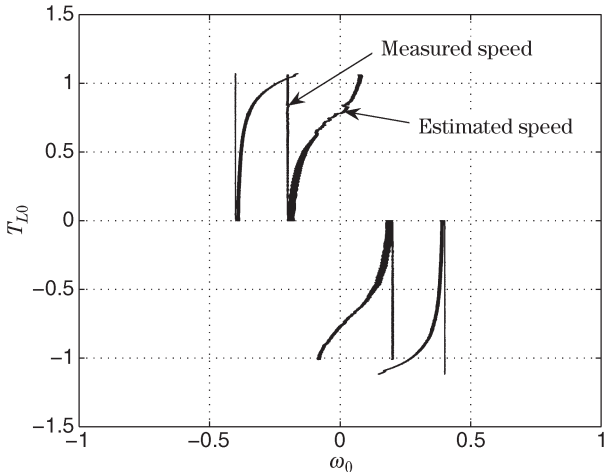

Fig. 9. Experimental results. Test in the regenerating mode in the $\{\omega_0, T_{L0}\}$ plane: $K_i = 1$, $K_p = 0$, and $G_s = G_r = 0$. Rotor speed is kept constant: $\omega_0 = -0.2$ and $\omega_0 = -0.4$ (quadrant 2) and $\omega_0 = +0.2$ and $\omega_0 = +0.4$ (quadrant 4). Ramp of load torque from 0 to 1 (quadrant 2) and from 0 to -1.5 (quadrant 4) during 100 s.

be aligned with D_2 to obtain the smallest unstable region. In this case, the determinant can be expressed as

$$\det(\widehat{A}_1) = \alpha \omega_{s0}^2 = 0. \tag{13}$$

III. STABILIZATION USING FEEDBACK GAINS G_s AND G_r

In this section, several designs leading to condition (13) are studied. In [6], the authors have proposed the particular structure $G_s = \begin{bmatrix} g_{sd} & -g_{sq} \\ g_{sq} & g_{sd} \end{bmatrix}$, $G_r = \begin{bmatrix} g_{rd} & 0 \\ 0 & g_{rd} \end{bmatrix}$, and $\phi = 0$. Considering $K_p = 0$, the condition $\det(\widehat{A}_1) = 0$ leads to

$$\det(\widehat{A}_1) = K\omega_{s0} \{\omega_{s0} [L_M(R_s + R_R + g_{sd}L_\sigma) + R_R L_\sigma]$$
$$- \omega_0(L_M R_s + L_M g_{sd}L_\sigma + L_M g_{rd})$$
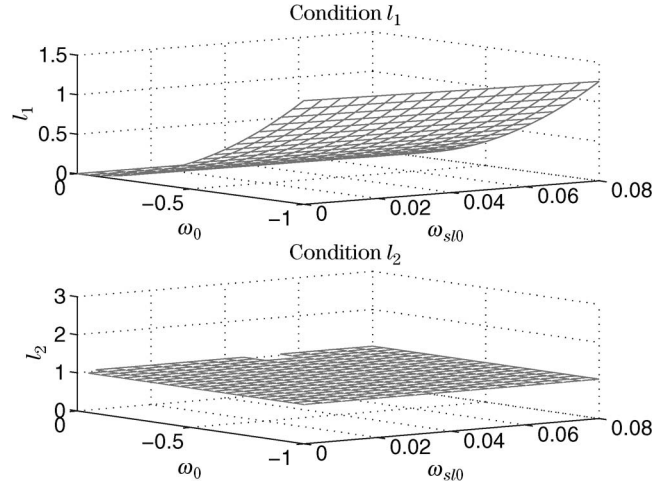$$+ R_R L_\sigma g_{sq}\}$$
$$= 0 \tag{14}$$

Fig. 10. Conditions l_1 and l_2: $-1 < \omega_0 < 0$ and $0 < \omega_{\text{sl0}} < 0.08$.

with $K = -(K_i \psi_{\text{ref}}^2 / L_M L_\sigma^2)$. The first solution is $\omega_{s0} = 0$, defining line D_2. The second term of the product depends on feedback gain G_r and defines line D_1 to be superposed on D_2 by calculating g_{rd}, g_{sd}, and g_{sq}. A solution is

$$\begin{cases} g_{rd} = -R_s \\ g_{sd} = kR_R/L_M \\ g_{sq} = k\omega_0, \qquad \text{where } k > 0. \end{cases} \tag{15}$$

This solution is close to the solution proposed in [6] with a five-parameter model. By inserting (15) in (14), we find

$$\det(\widehat{A}_1) = K\omega_{s0}^2 [L_M R_s + L_M R_R + (k+1)R_R L_\sigma] = 0 \tag{16}$$

which confirms that the proposed design allows alignment of D_1 with D_2. Theoretically, this observer is stable in all operating point except $\omega_s = 0$ if parameters are perfectly known. This stabilization can be verified by using conditions of complete stability (39). In Fig. 10, conditions l_1 and l_2 are plotted for -1 p.u. $< \omega_0 < 0$ and $0 < \omega_{\text{sl0}} < 0.08$ p.u. It leads to positive values in all the considered domains in the regenerating mode.

In practice, the term g_{sq} depends on ω_0 which is unrealistic because, in sensorless control, the actual speed is not available. Then, ω_0 is replaced with $\widehat{\omega}_0$, considering that the estimated speed tracks the real speed closely. Consequently, due to this approximation, the proof of global stability cannot be guaranteed. Therefore, an equivalent expression independent of ω_0 must be found. Let us consider an operating point in the vicinity of D_2 leading to $\omega_{s0} \approx 0$. In this case, the previous design becomes

$$\begin{cases} g_{rd} = -R_s \\ g_{sd} = kR_R/L_M \\ g_{sq} = k\omega_0 = k(\omega_{s0} - \omega_{\text{sl0}}) \approx -k\omega_{\text{sl0}}, \quad \text{with } k > 0 \end{cases} \tag{17}$$

which is independent of ω_0. By inserting (17) in (14), it holds that

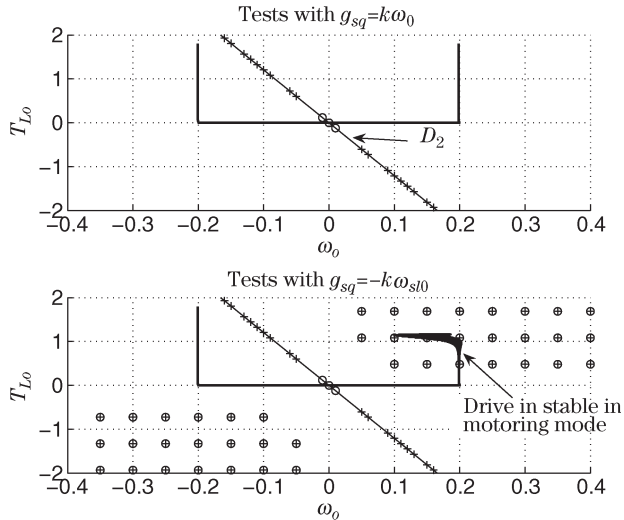$$\det(\widehat{A}_1) = K\omega_{s0}^2(L_M R_s + L_M R_R + R_R L_\sigma) = 0. \tag{18}$$

Fig. 11. Simulation results. Top: tests in the regenerating mode in the $\{\omega_0, T_{L0}\}$ plane, where $K_i = 1$, $K_p = 0$, $G_s = 0$, and G_r as in (15). Bottom: G_r as in (17) at the bottom. Rotor speed is kept constant: $\omega_0 = -0.1$ and $\omega_0 = -0.2$ (quadrant 2) and $\omega_0 = +0.1$ and $\omega_0 = +0.2$ (quadrant 4). Ramp of load torque from 0 to 1.5 (quadrant 2) and from 0 to -1.5 (quadrant 4) during 20 s.

Moreover, with $\omega_{slo} = R_R(i_{sqo}/\psi_{\mathrm{ref}})$ and $\psi_{\mathrm{ref}} = L_M i_{sdo}$, gain g_{sq} can be expressed as

$$g_{sq} = -k\frac{R_R}{L_M}\frac{i_{sqo}}{i_{sdo}}. \tag{19}$$

The feedback gains in (17) are replaced in (38) in order to derive the UEVs. Results are shown in Fig. 11, with corresponding simulations for both feedback gains (15) and (17). In both cases, the drive is stable in the regenerating mode, confirming that the unstable region is reduced to line D_2. Note that new unstable regions are emerging in the motoring mode for solution (17). Fig. 12 shows tests for varying stator resistance. The design (15) provides a closed loop that is very sensitive to parameter variations. In the first case [Fig. 12(a)], the stator resistance used in (2) is equal to the nominal value $R_{\mathrm{sobs}} = R_s$. The observer is stable as expected. In the second case [Fig. 12(b)], a $+3\%$ error is imposed on the stator resistance R_{sobs}. In this case, the observer is very sensitive and becomes unstable despite of the small error.

In the following, a feedback gain independent of ω_0 is sought [5]. An appropriate structure is $G_s = 0$, $G_r = \begin{bmatrix} g_{rd} & -g_{rq} \\ g_{rq} & g_{rd} \end{bmatrix}$, and $\phi = 0$. With $K_p = 0$, the condition $\det(\widehat{A}_1) = 0$ leads to

$$\det(\widehat{A}_1) = -\frac{K_i \psi_{\mathrm{ref}}^2}{L_M L_\sigma^2}\omega_{s0}\left[\omega_{s0}(L_M R_s + L_M R_R + L_M L_\sigma) + \omega_0(-L_M R_s - L_M g_{rd}) + R_R g_{rq}\right] = 0. \tag{20}$$

The first solution is $\omega_{s0} = 0$, defining line D_2. The second term of the product depends on feedback gain G_r and defines a line D_1 to be aligned with D_2 by calculating g_{rq} and g_{rd}. An obvious solution leading to (13) is

$$\begin{cases} g_{rq} = 0 \\ g_{rd} = -R_s. \end{cases} \tag{21}$$

Note that, for the inverse choice $G_r = 0$, $G_s = \begin{bmatrix} g_{sd} & -g_{sq} \\ g_{sq} & g_{sd} \end{bmatrix}$, $\phi = 0$, and $K_p = 0$, an equivalent condition to (15) is

$$\begin{cases} g_{sq} = 0 \\ g_{sd} = -\frac{R_s}{L_\sigma}. \end{cases} \tag{22}$$

This design is similar to the proposal in [4] ($g_{sd} = -0.25R_s$). Simulation tests with nominal parameters provide the same results as those shown on the top of Fig. 11. Therefore, the unstable region is again reduced to D_2 but with a feedback gain G which is now independent of the real speed w. Unfortunately, the design (21) leads to a system that is marginally stable. This observer is not applicable in a real context where parameters are not well known. Tests with stator variations lead to similar results as those shown in Fig. 12.

Both studied cases show the difficulty to design a feedback gain reducing the unstability region to D_2 and providing a robust EV placement robust to parameter variations. In the following, the reduction of the unstable region to D_2 is performed by acting on the speed adaptation law. By this way, the feedback gain can be used for an eventual robust EV placement.

IV. STABILIZATION USING ADAPTATION LAW

A. Design of the Speed Adaptation Law

In this section, a modified speed adaptation law is determined in order to reduce unstable regions to the line D_2. Several adaptive observers use a modified adaptation law in order to stabilize state estimation in the regenerating mode. The most general law is obtained by adding a complex number in the estimated speed equation [9].

$$\begin{cases} \frac{d}{dt}\widehat{\underline{i}}_s = -\left(\frac{1}{\tau_\sigma'} + j\omega_s\right)\widehat{\underline{i}}_s + \frac{1}{L_\sigma}\left(\frac{1}{\tau_R} - j\widehat{\omega}\right)\widehat{\underline{\psi}}_R + \frac{1}{L_\sigma}\underline{u}_s \\ \frac{d}{dt}\widehat{\underline{\psi}}_R = R_R\widehat{\underline{i}}_s - \left(\frac{1}{\tau_R} + j\widehat{\omega}_{s_l}\right)\widehat{\underline{\psi}}_R \\ \frac{d}{dt}\widehat{\omega} = -K_i\Im\left\{e^{-j\phi}\underline{e}_i\widehat{\underline{\psi}}_R^*\right\}. \end{cases} \tag{23}$$

Considering that $e^{-j\phi} = \cos\phi - j\sin\phi$, $\widehat{\psi}_{Rq} = 0$, and $\widehat{\psi}_{Rd} = \psi_{\mathrm{ref}}$, we find

$$\Im\left\{e^{-j\phi}\underline{e}_i\widehat{\underline{\psi}}_R^*\right\} = \psi_{\mathrm{ref}}(\cos\phi.e_{iq} - \sin\phi.e_{id}). \tag{24}$$

After linearization, the error state matrix $\widehat{A}_1$ becomes

$$\widehat{A}_1 = \begin{pmatrix} -\frac{1}{\tau_\sigma'} & +\omega_{s0} & \frac{1}{\tau_R L_\sigma} & +\frac{\omega_0}{L_\sigma} & 0 \\ -\omega_{s0} & -\frac{1}{\tau_\sigma'} & -\frac{\omega_0}{L_\sigma} & +\frac{1}{\tau_R L_\sigma} & -\frac{\psi_{\mathrm{ref}}}{L_\sigma} \\ R_R & 0 & -\frac{1}{\tau_R} & +\omega_{sl0} & 0 \\ 0 & R_R & -\omega_{sl0} & -\frac{1}{\tau_R} & \psi_{\mathrm{ref}} \\ -K_i\psi_{\mathrm{ref}}\sin\phi & K_i\psi_{\mathrm{ref}}\cos\phi & 0 & 0 & 0 \end{pmatrix}. \tag{25}$$

For $\phi = 0$, (25) is equivalent to (38) with $G_s = G_r = 0$ and $K_p = 0$. As in Section III, the parameter ϕ reducing the
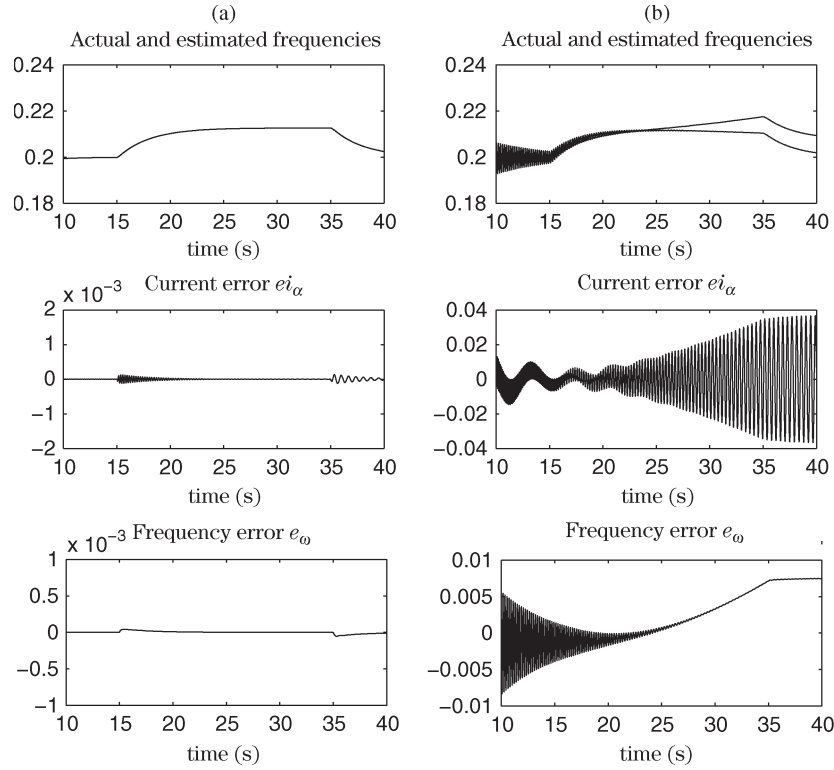
Fig. 12. Simulation results. Test in the regenerating mode: $K_i = 1$, $K_p = 0$, and G_s and G_r as in (15). Rotor speed is kept constant: $\omega_0 = +0.2$ (quadrant 4). Ramp of load torque from 0 to -1.5 (quadrant 4) during 20 s at $t = 15$ s. (a) $R_{\mathrm{sobs}} = R_s$. (b) $R_{\mathrm{sobs}} = 1.03 R_s$. Errors are expressed in the fixed reference frame.

unstable region to the inobservability line D_2 is sought. The stability limits are defined by $\det(\widehat{A}_1) = 0$ with

$$\det(\widehat{A}_1) = -\frac{K_i \widehat{\psi}_o^2 \omega_{so}}{L_M L_\sigma^2} Z \qquad (26)$$

where

$$Z = \omega_{s0} \left[\cos\phi(L_M R_s + R_R L_\sigma + R_R L_M) - \sin\phi L_M L_\sigma \omega_{\mathrm{sl0}}\right]$$
$$- \cos\phi L_M R_s \omega_0 + \sin\phi R_R R_s. \qquad (27)$$

The first solution is $\omega_{s0} = 0$, defining line D_2. The angle ϕ must be calculated first to transform Z into a line (D_1) and second to superpose D_1 on D_2. The proposed solution allows elimination of the term $\sin\phi R_R R_s - \cos\phi L_M R_s \omega_o$ by choosing

$$\phi_{\mathrm{opt}} = \tan^{-1}\left(\frac{\omega_0 L_M}{R_R}\right). \qquad (28)$$

The corresponding regions of instability can be derived by substituting (28) in (27). The determinant (26) becomes

$$\det(\widehat{A}_1) = K\omega_{so}^2 \left[L_M R_R R_s + L_M R_R^2 \right.$$
$$\left. + L_\sigma R_R^2 - L_M^2 L_\sigma \omega_0 \omega_{\mathrm{sl0}}\right]. \qquad (29)$$

Let us consider a domain where

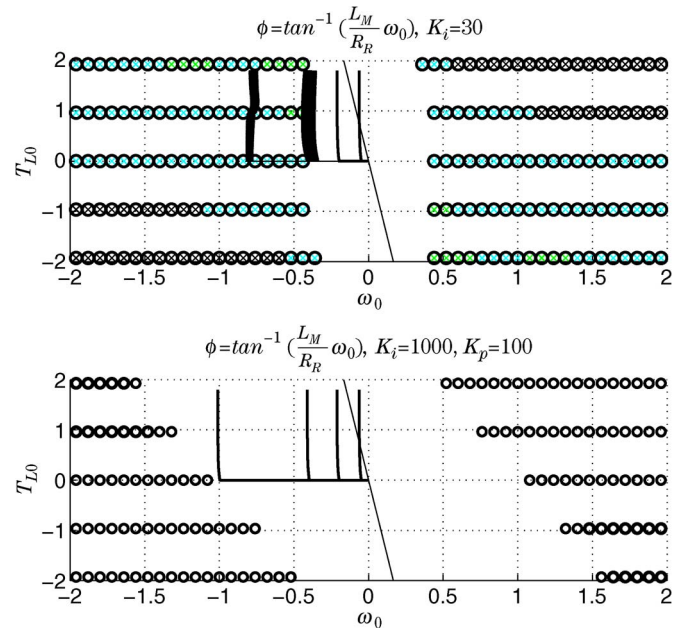$$L_M^2 L_\sigma \omega_0 \omega_{\mathrm{sl0}} \ll L_M R_R R_s + R_R^2(L_M + L_\sigma). \qquad (30)$$

Fig. 13. Simulation results. Tests in the regenerating mode in the $\{\omega_0, T_{L0}\}$ plane for different values of parameters K_i and K_p: $\phi = \phi_{\mathrm{opt}}$. Rotor speed is kept constant. Ramp of load torque from 0 to 1.5 (quadrant 2) during 20 s. Top: $K_i = 30$. Bottom: $K_i = 1000$ and $K_p = 100$. Markers "o" locate unstable regions.

In this region of the $\{\omega_0, \omega_{\mathrm{sl0}}\}$ plane, the determinant $\det(\widehat{A}_1)$ is expressed as (13), and the observer can be considered as stable. Top of Fig. 13 shows in the same plot the unstable EV corresponding to the design ϕ_{opt} in the $\{\omega_0, T_{L0}\}$
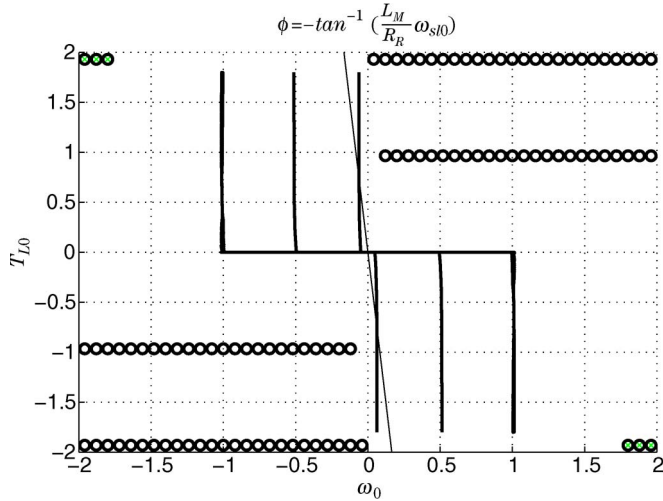
Fig. 14. Simulation results. Tests in the regenerating mode in the $\{\omega_0, T_{L0}\}$ plane for $\phi_{\mathrm{opt}} = -\tan^{-1}(\omega_{\mathrm{sl0}} L_M / R_R)$ plane. Rotor speed is kept constant. Ramp of load torque from 0 to 1.5 (quadrant 2) during 20 s: $K_i = 30$. Markers "o" locate unstable regions.

Fig. 15. Experimental results: $\phi_{\mathrm{opt}} = -\tan^{-1}(i_{sqo}/i_{sdo})$. Tests in the regenerating mode in the $\{\omega_0, T_{L0}\}$ plane: $K_i = 1$, $K_p = 0$, and $G_s = G_r = 0$. Rotor speed is kept constant: $\omega_0 = -0.2$ and $\omega_0 = -0.4$ (quadrant 2) and $\omega_0 = +0.2$ and $\omega_0 = +0.4$ (quadrant 4). Ramp of load torque from 0 to 1 (quadrant 2) and from 0 to -1.5 (quadrant 4) during 100 s.

plane and tests at constant speed with increasing load torque. In a restricted domain, unstable regions in the regenerating mode are reduced to the line $\omega_{s0} = 0$. In the motoring mode, unstable regions appear, while this was not the case for $\phi = 0$ (see Fig. 1). It confirms that ϕ must be chosen as $\phi = 0$ in the motoring mode and $\phi \neq 0$ in the regenerating mode [9]. The stable region can be increased, making $K_p \neq 0$, as shown at the bottom of the figure.

As discussed in the design described in Section III, the angle (28) can be expressed using only measured signals

$$\phi_{\mathrm{opt}} \approx -\tan^{-1}\left(\frac{\omega_{\mathrm{sl0}} L_M}{R_R}\right) \qquad (31)$$

i.e.,

$$\tan(\phi_{\mathrm{opt}}) = -\frac{i_{sqo}}{i_{sdo}}. \qquad (32)$$

Finally, the solution is

$$\phi_{\mathrm{opt}} = -\tan^{-1}\left(\frac{i_{sqo}}{i_{sdo}}\right). \qquad (33)$$

In conclusion, ϕ_{opt} can be approximated by the angle of the current phasor $\underline{i}_s$ in the synchronous rotating reference frame. From (24), the new speed adaptation law is now defined by

$$\frac{d}{dt}\widehat{\omega} = -K_i \frac{\psi_{\mathrm{ref}}}{\|\underline{i}_{so}\|}(i_{sd} e_{iq} - i_{sq} e_{id}) \qquad (34)$$

with $\|\underline{i}_{so}\| = \sqrt{i_{sdo}^2 + i_{sqo}^2}$.

The corresponding unstable EVs and tests at constant speed with increasing load torque are simultaneously shown in Fig. 14. In comparison with the solution (28), the stable domain is increased. These tests lead to stable operations in the regenerating mode. Corresponding experimental results are shown
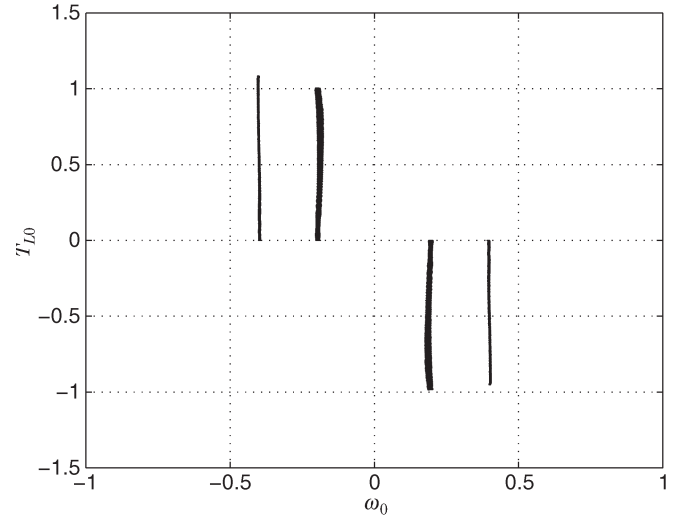
in Fig. 15. In comparison with Fig. 9, the stabilization can be verified. However, these results are obtained with a good tuning of the stator resistance. In some cases, this resistance must be intentionally overestimated to achieve stability, as mentioned in [9].

B. Analysis of a Similar Design

In [8], the proposed speed adaptation law uses the term ϵ, which is defined by

$$\epsilon = \Im\left\{\underline{e}_i \widehat{\underline{\psi}}_r^*\right\} + k\Re\left\{\underline{e}_i \widehat{\underline{\psi}}_r^*\right\} \qquad (35)$$

with k as a parameter to be determined. By expressing (35) in component form and after linearization, the following state error matrix is obtained:

$$\widehat{A}_1 = \begin{pmatrix} -\frac{1}{\tau_\sigma'} & +\omega_{s0} & \frac{1}{\tau_R L_\sigma} & +\frac{\omega_0}{L_\sigma} & 0 \\ -\omega_{s0} & -\frac{1}{\tau_\sigma'} & -\frac{\omega_0}{L_\sigma} & +\frac{1}{\tau_R L_\sigma} & -\frac{\psi_{\mathrm{ref}}}{L_\sigma} \\ R_R & 0 & -\frac{1}{\tau_R} & +\omega_{\mathrm{sl0}} & 0 \\ 0 & R_R & -\omega_{\mathrm{sl0}} & -\frac{1}{\tau_R} & \psi_{\mathrm{ref}} \\ kK_i\psi_{\mathrm{ref}} & K_i\psi_{\mathrm{ref}} & 0 & 0 & 0 \end{pmatrix}. \qquad (36)$$

It is easy to see that (36) is a particular case of (25) with a small ϕ. In this case, $\cos\phi \to 1$, and $\sin\phi \to \phi$; then, $k = \lim(\phi)_{\phi \to 0}$. From (28), it holds

$$k = \lim(\phi_{\mathrm{opt}})_{\phi_{\mathrm{opt}} \to 0} = -\frac{L_M \omega_0}{R_R}. \qquad (37)$$

This parameter is equivalent (in a four-parameter representation) to the gain proposed by Rashed *et al.* By replacing (37) in (36), unstable EVs can be calculated. The resulting unstable regions in the $\{\omega_0, T_{L0}\}$ plan are close to those shown in Fig. 14.

$$\widehat{A}_1 = \begin{pmatrix} -\frac{1}{\tau_\sigma'} - g_{s_d} & +\omega_{s0} + g_{s_q} & \frac{1}{\tau_R L_\sigma} & +\frac{\omega_0}{L_\sigma} & 0 \\ -\omega_{s0} - g_{s_q} & -\frac{1}{\tau_\sigma'} - g_{s_d} & -\frac{\omega_0}{L_\sigma} & +\frac{1}{\tau_R L_\sigma} & -\frac{\psi_{\text{ref}}}{L_\sigma} \\ R_R - g_{r_d} & +g_{r_q} & -\frac{1}{\tau_R} & +\omega_{\text{sl}0} & 0 \\ -g_{r_q} & R_R - g_{r_d} & -\omega_{\text{sl}0} & -\frac{1}{\tau_R} & \psi_{\text{ref}} \\ A_{51} & A_{52} & A_{53} & A_{54} & A_{55} \end{pmatrix} \tag{38}$$

where

$$A_{51} = \psi_{\text{ref}} \sin\phi \left[K_i - K_p (R_s + R_R)/L_\sigma \right] - K_p \psi_{\text{ref}} \omega_{s0} \cos\phi$$

$$A_{52} = \psi_{\text{ref}} \cos\phi \left[K_i - K_p (R_s + R_R)/L_\sigma \right] + K_p \psi_{\text{ref}} \omega_{s0} \sin\phi$$

$$A_{53} = -K_p \psi_{\text{ref}} \omega_0 \cos\phi/L_\sigma + K_p \psi_{\text{ref}} \sin\phi R_R/L_M L_\sigma$$

$$A_{54} = K_p \psi_{\text{ref}} \cos\phi R_R/L_M L_\sigma + K_p \psi_{\text{ref}} \omega_0 \sin\phi/L_\sigma,$$

$$A_{55} = -K_p \psi_{\text{ref}}^2 \cos\phi/L_\sigma.$$

$$B_1 = \begin{pmatrix} +e_{i_{q0}} & +\frac{1}{L_\sigma} e_{\psi_{q0}} \\ -e_{i_{d0}} & -\frac{1}{L_\sigma} e_{\psi_{d0}} \\ +e_{\psi_{q0}} & -e_{\psi_{q0}} \\ -e_{\psi_{d0}} & e_{\psi_{d0}} \end{pmatrix}$$

$$\begin{cases} l_1 = \frac{(g_{sd}L_\sigma + g_{rd} + R_s)(a + \omega_0 \tan\phi) + (g_{sq}L_\sigma + g_{rq} + (\omega_0 + \omega_{\text{sl}0})L_\sigma)(\omega_0 - a.\tan\phi)}{g_{sd}L_\sigma + (R_R + R_s) - (g_{sq} + \omega_{\text{sl}0} + \omega_0)L_\sigma L_M \tan\phi} > 0, \\ l_2 = \frac{(\omega_0 + \omega_{\text{sl}0})[(g_{sd} + a)Lfn - (\omega_{\text{sl}0} + g_{sq})L_\sigma \tan\phi + (R_R + R_s)] + (g_{sq}L_\sigma + g_{rq})(a + \omega_0 \tan\phi) - (g_{sd}L_\sigma + g_{rd} + R_s)(\omega_0 - a.\tan\phi)}{(\omega_0 + \omega_{\text{sl}0})(g_{sd}L_\sigma + (R_R + R_s) - (g_{sq} + \omega_{\text{sl}0} + \omega_0)L_\sigma \tan\phi)} > 0 \end{cases} \tag{39}$$

where $a = (R_R/L_M)$

V. CONCLUSION

This paper has presented stability conditions of full adaptive observers in the regenerating mode. It has been shown that observer stability can be interpreted as the restriction of the unstable region to the inobservability line $\omega_s = 0$. Moreover, a criterion defining stability limits has been proposed. Its main interest is the design of stabilizing feedback gains or speed adaptation laws. A correct use of this criterion can be resumed as follows.

1) Calculate the determinant $\det(A_1)$, including gain G and/or parameters ϕ under literal form.
2) Find the design leading to the condition $\det(\widehat{A}_1) = \alpha \omega_{s0}^2 = 0$ if it exist.
3) Calculate A_1's EV, taking into account stabilizing gain G and/or parameters ϕ.
4) Represent UEV in the $\{\omega_0, T_{L0}\}$ plane.

The most popular designs lead to the sought region reduction. However, in many cases, observer stability is very parameter dependent. In particular, it seems difficult to design a feedback gain allowing either region reduction or a robust EV placement. From our experience, this sensitivity does not allow exploitable experimental results. In particular, any reproducibility can be obtained because the required precision on parameter knowl-

edge (few percent for R_s) cannot be held for a long time without additional compensation systems. With the proposed method, the stability of simultaneous estimation of speed and stator resistance can be easily performed. Without resistance estimation, the most reasonable way seems to be the following.

1) The reduction of the unstable region in the regenerating mode by an appropriate design of the parameter ϕ.
2) The design of a robust EV placement in order to make the observer as insensitive of R_s variations as possible. The idea would be to exploit the conditions of positive realness proposed in [11] but using a Lyapunov inequality rather than equality. More precisely, it could be interesting to consider the Linear Matrix Inequality (LMI) version of the positive real lemma [15]. Indeed, the LMI approach is adapted in the presence of parametric uncertainty (such as R_s), particularly through the polytopic description [16]–[18].

REFERENCES

[1] H. Kubota and K. Matsuse, "DSP-based speed adaptive flux observer of induction motor," *IEEE Trans. Ind. Appl.*, vol. 29, no. 2, pp. 344–348, Mar./Apr. 1993.
[2] G. Yang and T. Chin, "Adaptive-speed identification scheme for a vector-controlled speed sensorless inverter-induction motor drive," *IEEE Trans. Ind. Appl.*, vol. 29, no. 4, pp. 820–825, Jul./Aug. 1993.

[3] G. Kubota, L. Sato, Y. Tamura, K. Matsume, H. Ohta, and Y. Hori, "Stable operation of adaptive observer based sensorless induction motor drives in regenerating mode at low speeds," in *Conf. Rec. IEEE IAS Annu. Meeting*, 2001, pp. 469–474.

[4] S. Suwankawin and S. Sangwongwanich, "A speed-sensorless IM drive with decoupling control and stability analysis of speed estimation," *IEEE Trans. Ind. Electron.*, vol. 49, no. 2, pp. 444–455, Apr. 2002.

[5] N. Bensiali, C. Chaigne, and E. Etien, "Optimal observer design for sensorless control of induction motor in regenerating-mode," in *Conf. Rec. IEEE SPEEDAM*, 2006, pp. 996–1001.

[6] S. Suwankawin and S. Sangwongwanich, "Design strategy of an adaptive full-observer for speed-sensorless induction-motor drives-tracking performance and stabilization," *IEEE Trans. Ind. Electron.*, vol. 53, no. 1, pp. 96–119, Feb. 2006.

[7] H. Tajima and G. Guidi, "Consideration about problems and solutions of speed estimation method and parameter tuning for speed-sensorless vector control of induction motor drives," *IEEE Trans. Ind. Appl.*, vol. 38, no. 5, pp. 1282–1289, Sep./Oct. 2002.

[8] M. Rashed, F. Stronach, and P. Vas, "A stable MRAS-based sensorless vector control induction motor drive at low speeds," in *Conf. Rec. IEEE IEMDC*, 2003, pp. 139–144.

[9] M. Hinkkanen, "Stabilization of regenerating-mode operation in sensorless induction motor drives by full-order flux observer design," *IEEE Trans. Ind. Electron.*, vol. 51, no. 6, pp. 1318–1328, Dec. 2004.

[10] L. Harnefors, "Globally stable speed-adaptive observers for sensorless induction motor drives," *IEEE Trans. Ind. Electron.*, vol. 54, no. 2, pp. 1243–1245, Apr. 2007.

[11] S. Sangwongwanich, S. Suwankawin, S. Po-ngam, and S. Koonlaboon, "A unified speed estimation design framework for sensorless AC motor drives based on positive-real property," in *Conf. Rec. Power Conversion Conf.*, Nagoya, Japan, 2007, pp. 1111–1118.

[12] L. Harnefors and M. Hinkannen, "Complete stability of reduced-order and full-order observers for sensorless IM drives," *IEEE Trans. Ind. Electron.*, vol. 55, no. 3, pp. 1319–1329, Mar. 2008.

[13] K. Ohyama, G. M. Asher, and M. Sumner, "Comparative analysis of experimental performance and stability of sensorless induction motor drives," *IEEE Trans. Ind. Electron.*, vol. 53, no. 1, pp. 178–186, Feb. 2006.

[14] M. Hinkkanen, "Parameter sensitivity of full-order flux observers for induction motor," *IEEE Trans. Ind. Appl.*, vol. 39, no. 4, pp. 1127–1135, Jul./Aug. 2003.

[15] S. Boyd, L. El Ghaoui, E. Ferron, and V. Balakrishnan, *Linear Matrix Inequalities in System and Control Theory*. Philadelphia, PA: SIAM, 1994.

[16] D. Peaucelle, D. Arzelier, O. Bachelier, and J. Bernussou, "A new robust D-stability condition for real convex polytopic uncertainty," *Syst. Control Lett.*, vol. 40, no. 1, pp. 21–30, May 2000.

[17] O. Bachelier, D. Henrion, B. Pradin, and D. Mehdi, "Robust root-clustering in unions or intersections of regions," *SIAM J. Control Optim.*, vol. 43, no. 3, pp. 1078–1093, 2004.

[18] J. Bosche, O. Bachelier, and D. Mehdi, "An approach for robust matrix root-clustering analysis in a union of regions," *IMA J. Math. Control Inf.*, vol. 22, no. 3, pp. 227–239, Sep. 2005.

Erik Etien was born in France in 1970. He received the Ph.D. degree in automatic control from the University of Poitiers, Poitiers, France, in 1999.

His research interests include the development of soft sensors in the field of electrical engineering.

Claude Chaigne was born in 1959. He received the Ph.D. degree in automatic control from the University of Poitiers, France, in 2009.

His major fields of interest in research include field oriented control drives of induction machines associated with field programmable gate array (FPGA) based real-time control systems.

Nadia Bensiali was born in Algeria in 1971. She received the Engineering and DEA degrees from the School of Engineering, University Badji Mokhtar, Annaba, Algeria, in 1994 and 1997, respectively.

Her major fields of research include the sensorless control of induction motors.